ABSTRACT

Automated Enrichment of Single-Walled Carbon Nanotubes with Optical Studies of Enriched Samples

by

Griffin Canning

The design and performance of an instrument is presented whose purpose is the extraction of samples highly enriched in one species of single-walled carbon nanotubes from density gradient ultracentrifugation. This instrument extracts high purity samples which are characterized by various optical studies. The samples are found to be enriched in just a few species of nanotubes, with the major limitation to enrichment being the separation, rather than extraction. The samples are then used in optical and microscopic studies which attempt to determine the first absorption coefficient (S_1) of the (*6,5*) species of nanotube. Initial experiments give a value of 9.2 ± 2.6 cm^2 C $atom^{-1}$. Future work is proposed to improve upon the experiment in an attempt to reduce possible errors.

ACKNOWLEDGEMENTS

Khanssaa El Alami El Aroussi
for her support and inspiration

My family
for providing me the opportunity to begin this journey

Dr. R. Bruce Weisman
for his ability to ask the important question, is it viable and valuable?

Dr. Sergei Bachilo
for immeasurable guidance in how to answer that important question

Mr. Jason Streit
for always listening when my ideas needed vocalization

Dr. Saunab Ghosh
without whose dedication and work my research would be impossible

Table of Contents

Table of Figures

1. Introduction

Although it is generally held that carbon nanotubes were discovered by Iijima in 1991 at NEC,[1] carbon nanotubes had been first seen but not characterized in 1952 by two scientists who published their results in a Russian journal.[2] Regardless of when they were discovered, scientists have become extremely interested in carbon nanotubes within the last two decades. Much of this interest is focused on Single Walled Carbon Nanotubes (SWCNTs), owing to their unique and useful mechanical and thermal properties and their promise for applications in electronic materials[3].

The structure of SWCNTs can be imagined to be a flat sheet of graphene that has been rolled up to form a crystalline tube, as shown in figure 1. Each roll-up vector, labeled with two indices, *n* and *m*, corresponds to a different tube species with a different diameter. When the sheet of graphene is rolled up along this vector, the unit cells will align along the length of the tube. This creates a nanotube with a crystalline structure along the screw axis.

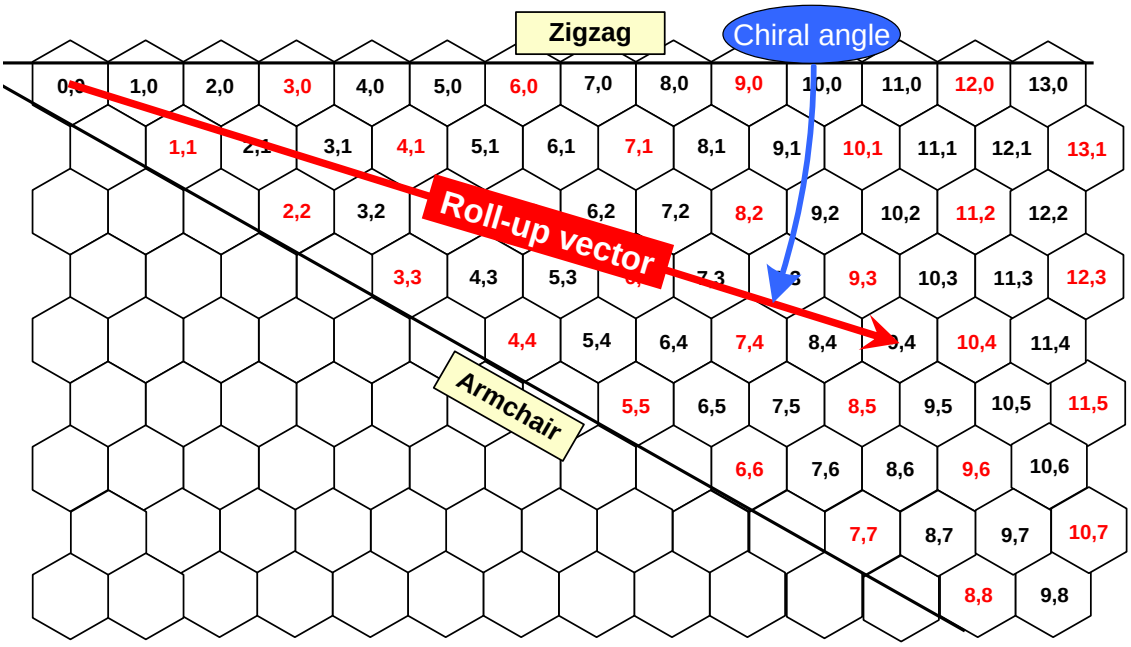

Figure 1: Cartoon depicting the "rolling up" of a graphene sheet to form a SWCNT.[4] Each (*n*,*m*) index is a different chemical species.

Since these tubes are quasi one-dimensional crystals, their energy can be described by:

$$\varepsilon = \varepsilon_i + \frac{\hbar^2 k^2}{2m} \tag{1}$$

where ε_i is the energy of the eigenstate of the radial part of the wavefunction and k is the wavevector along the tube axis. The density of states is then given by

$$D(\varepsilon) = \sum_i D_i(\varepsilon) \tag{2}$$

where

$$D_i(\varepsilon) = \alpha \frac{1}{(\varepsilon - \varepsilon_i)^{1/2}} \tag{3}$$

Therefore $D(\varepsilon)$ diverges when the electronic energy is equal to one of the quantized values which depend only on the radius. These divergences are known as van Hove singularities. A plot of the electronic structure of a SWCNT is shown in figure 2. Each species of nanotube has singularities at distinct energies, and therefore distinct optical properties. This serves to re-emphasize the need to consider each species of nanotube as a distinct chemical species within the chemical family of carbon nanotubes.

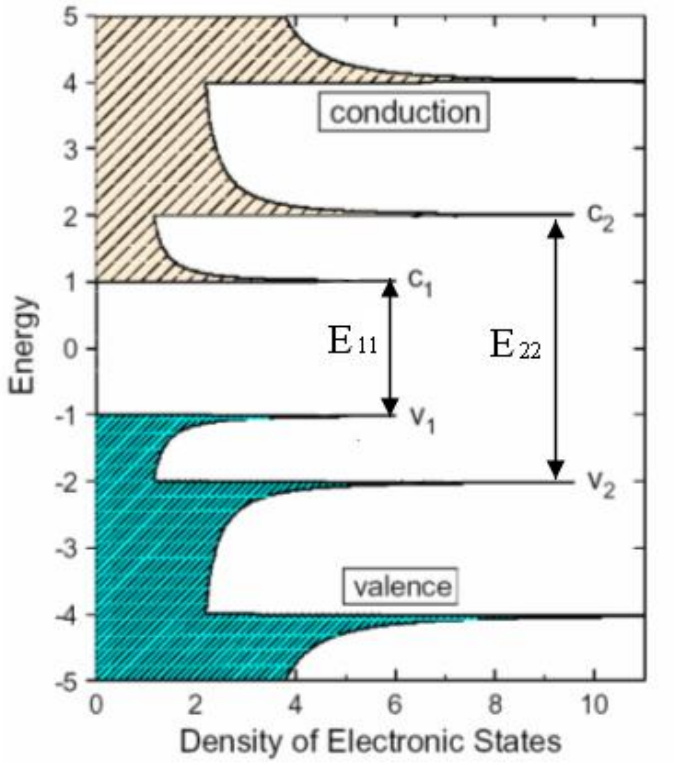

Figure 2. Density of states of semiconducting carbon nanotube, highlighting the electronic transitions used in optical studies.[4].

Tubes with a large (>>k_bT) gap between their first valence (V_1) and conduction (C_1) bands will absorb light at characteristic wavelengths to promote an electron from a valence band to its corresponding conduction band. This results in the creation of a bound electron-hole pair, called an exciton, which will diffuse along the length of the tube. These excitons relax very quickly into the lowest possible energy, with the electron in C_1 and the hole in V_1. The exciton will eventually recombine by emitting a photon. This fluorescence is a useful tool for performing optical studies on SWCNTs, since the characteristic wavelengths of absorbed and emitted photons are proportional to the diameter of the tube.

Unfortunately, current synthesis methods produce a mixture of different species of tubes, as well as impurities of metal catalysts and amorphic carbon. As purchased, a HiPco (High Pressure Carbon Monoxide method) sample can contain dozens of different species. This leads to serious obstacles to the precise optical study of SWCNTs, since without further purification; a spectrum of a bulk sample will contain many peaks which are difficult to resolve. For example, figure 3 shows a fluorescence spectra of the unenriched bulk sample used in this study.

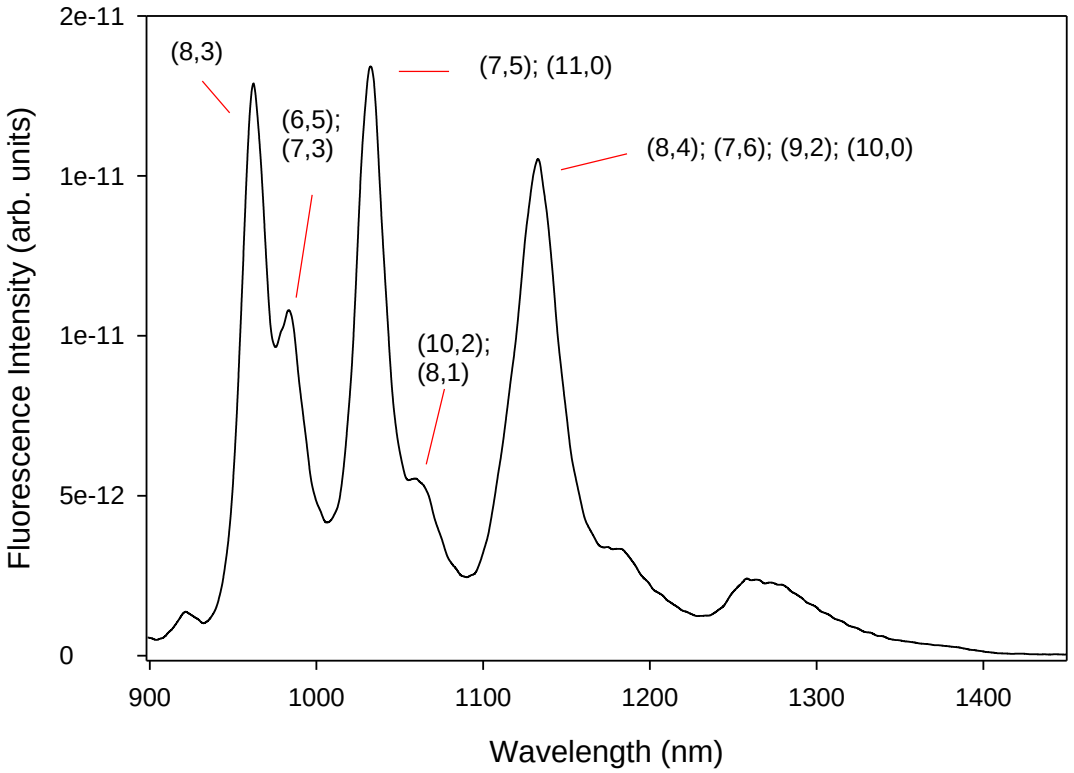

Figure 3. Fluorescence Intensity of a bulk sample of SWCNTs dispersed in sodium cholate. This spectra is typical of HiPco samples without purification, showing the limitation imposed by the current synthesis methods.

There are currently two well established methods for separating bulk carbon nanotube samples. The first is ion exchange chromatography of SWCNTs that have been wrapped in single stranded DNA made of alternating guanine and thymine base pairs.[5] The DNA-nanotube conjugate is passed through a strong anion exchange column where the anionic phosphate groups of the DNA interact with the column coating.

Due to diameter dependence of the wrapping angle, the linear charge density varies with tube species, causing the interaction strength between the DNA wrapped tubes and column to also vary with diameter. This method provides high quality separations, but unfortunately requires expensive synthetic DNA strands. Density gradient ultracentrifugation (DGU) is the other popular method for separating SWCNT samples.[6]

DGU has been applied in biology and biochemistry since the 1950's. Originally, it was used to separate lipids and proteins from serum. This lab has developed a technique to further improve the application of a DGU separation to nanotubes by employing a nonlinear density gradient.[7] This is explained in more detail in Appendix B. In essence, the technique begins by suspending the SWCNTs in solution by coating them with surfactant. A density gradient is then formed into which the tubes are injected. The sample is then subjected to ultracentrifugation, during which the tubes will migrate through the density gradient until they reach their isopycnic point, i.e. the point at which the density of the tube-surfactant object is equal to that of the surrounding medium. Each species of nanotube-surfactant micelle has a different density, which is directly related to the diameter of the nanotube species in question. Therefore, this separation produces colored bands of solution which are highly enriched in one type of SWCNT. A picture of a post-DGU sample is shown in figure 4.

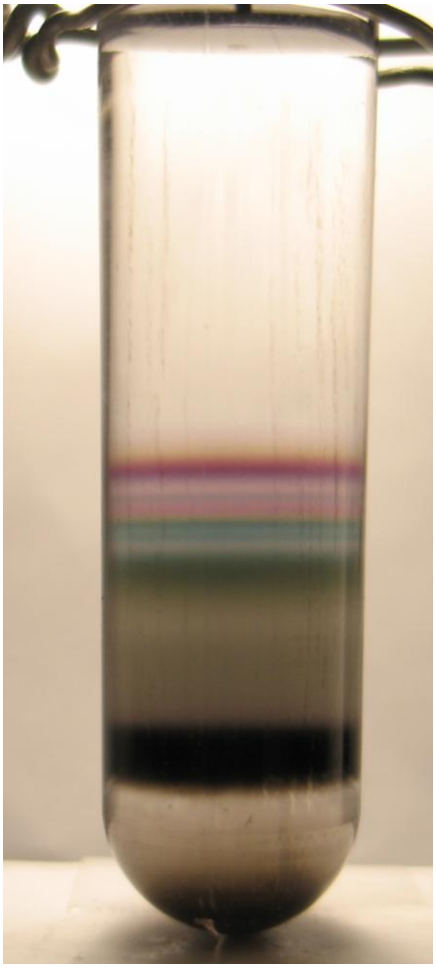

Figure 4. A picture of a DGU sample in which each of the colored bands is a distinct layer of sample enriched in a different species of SWCNT. The purple band near the top is the (*6,5*) band.

These samples can then be subjected to non-intrusive analysis techniques, such as absorption or fluorescence studies. If care is taken, data can be obtained for each layer independently of the others, allowing the experimenter to focus on one (*n,m*) species at a time. However, in order to subject one layer to any kind of invasive technique – defined as one that disturbs or mixes the sample – that layer must first be extracted from the post-DGU sample. Examples of this type of experiment would be functionalization, microscopy, or preparation for use as a component of a novel device. Early in the history of DGU, the density differences between target analytes were so large that this extraction

could easily be performed manually with a pipette. However, in the case of SWCNT separations, the density changes are relatively minor, with most SWCNT-surfactant micelles of interest predicted to fall somewhere in the rage of 1.05-1.08 g/cm^3.[8] Thus a higher degree of precision is required. Some automated instruments exist, but as they were designed for use with biological samples, their performance is unsatisfactory. In this study I present the design and performance of a novel instrument for collection of samples enriched in individual (*n*,*m*) species from a post-DGU separated sample. The samples obtained from this instrument will open new avenues of study for basic research applications.

One very important missing piece of the descriptive puzzle of nanotubes is the ability to determine the concentration of tubes in solution. The purpose of obtaining the concentration is manifold. Any kind of biological or environmental study will benefit greatly from this information, as the concentration of any medicine or toxic agent is required to determine its effect on the body. Indeed, many drugs become toxic (and *vice versa*) within specific concentration ranges. Beyond these concerns, it is important to understand the concentration of any chemical present in a solution reaction in order to fully characterize that solution.

One powerful and important tool in determining the concentration of chromophores is Beer's Law, $I/I_0 = e^{-\rho\sigma l}$ which states that the intensity of light transmitted through a sample, I, relative to the incident light intensity, I_0, is dependent upon the number density ρ of the chromophores present, the path length the light travels through the sample, l, and the absorption cross section of those chromophores, σ. The absorbance, given by the negative of the base 10 log of the transmission, and path length

are determined experimentally, while the absorption cross section is dependent on the chemical species and wavelength in question. When σ is known, it is simple to determine the concentration experimentally.

To date, five studies have reported the absorption cross section of (*6,5*) SWCNTs. These studies have produced varied results with poor agreement. The study by Islam, et al. was based on absorption studies conducted on a bulk sample of un-enriched nanotubes whose concentration is determined gravimetrically, and achieves a value for the absorption cross section of the second transition of ~0.8 x 10^{-18} cm^2 C $atom^{-1}$, one order of magnitude lower than the other three studies discussed.[9]

In work by Zheng and Diner, the authors utilized a highly effective method for separating their nanotubes. This method involves wrapping the nanotubes in synthetic, single-stranded DNA segments, and then passing these DNA-SWCNT complexes through an ion exchange chromatography column. Using the highly enriched samples they obtained, the authors dried, weighed and measured an absorbance spectrum for the DNA-SWCNT complexes. From this they estimated a mass to absorbance ratio which leads to an absorption cross section of 0.7 x 10^{-17} cm^2 C $atom^{-1}$ for the first transition.[10] However, the authors were forced to make serious assumptions both about the SWCNT mass percent of the DNA-SWCNT complex, and the percent composition of (*6,5*) nanotubes within their purified sample.

Berciaud et al. began by depositing nanotubes into an agarose gel. They then measured the kinetics of the luminescence decay following laser pulses. They used the kinetics in association with continuous wave absorption measurements to determine the absorption cross section. Their final result was ~1 x 10^{-17} cm^2 C $atom^{-1}$ for the S_2

transition[11]. One issue with this study is that their model does not account for any kind of nonlinear exciton recombination, such as exciton-exciton annihilation, which can occur at power levels one order of magnitude lower than that used in their study[12].

Finally, the most recent report by Schöppler et al. also attempted to measure the S_1 cross section of (*6,5*) nanotubes. The authors attempted two methods of SWCNT concentration determination. The first involved wrapping samples derived using Zheng's method for purification with DNA that had been tagged with a fluorophore, 6-carboxyfluorescein (FAM), whose optical properties were well known. The sample's fluorescence at FAM resonance wavelength was measured, which, when coupled with an estimate of the DNA:SWCNT stoichiometry, allowed them to estimate SWCNT concentration. The other method the authors used to determine the SWCNT concentration was vacuum filtration followed by AFM imaging to count the number of nanotubes. These differing methods produced two values, 2.3×10^{-17} and 1.1×10^{-17} cm^2 C $atom^{-1}$, which are not in close agreement[13].

In this thesis, I present the design, structure and performance of an instrument designed to extract samples enriched in single species of SWCNTs from DGU separations. I also present preliminary work on the determination of the absorption cross section of the (*6,5*) SWCNT species using samples obtained with my instrument. For this study, I will focus my attention on the first absorption peak, S_1. I count the total number density of SWCNTs in a known volume of sample, giving the concentration of SWCNTs in that sample. The concentration and absorption can be combined to calculate the absorption cross section for this species.

2. Instrumental Design - Fractionator

The goals for the Fractionator are determined by the DGU process which takes place before extraction. Post-DGU, the sample is separated into bands as described above. The Fractionator should then be capable of receiving this sample and extracting each band individually with minimal disturbance to other bands remaining in the sample tube. It should be capable of extracting multiple layers from one DGU sample while maintaining a high degree of enrichment and low mixing. It should also be capable of performing this extraction in an automated, computer-controlled manner with high speed and precision.

Our instrument is designed to be as precise as possible while maintaining the simplicity of manual extraction with a syringe. To that end, the instrument was designed with two different, independent instrumental systems. These are the Motion System and the Fluid System. The Motion System composed of a sample holder attached to three linear translation stages. The motors are commanded by three corresponding controllers which provide very steady, fine grain 3-dimensional spatial control of the sample position. The Fluid System is made up of a computer-controlled syringe pump, microbore Tygon tubing, a 3-way electrical pinch valve, and small diameter needles for insertion into and dispensing of the sample. This system provides slow, stable extraction of the sample which minimizes disturbance of the layering of the sample while maximizing total extracted volume.

As previously described, the Motor Control system is based on three stepper motor driven translation stages, model VT-80 manufactured by Micos GmbH. The VT-80

model has 200 steps per millimeter of linear motion, and is capable of splitting each step into 2, 4, 8, 16, 32, or 64 microsteps. Micos reports that these motors have a typical resolution of 0.2 μm. Each motor is controlled by a corresponding stepper motor controller, which is capable of varying the speed, acceleration, stepping mode (i.e. the number of microsteps per step), direction and distance of travel for the sample stage mounted on the motor. The motors are combined such that the Y motor translates the X motor, which in turn translates the Z motor, to which the sample holder is attached. In this way, 3-dimensional control is achieved. A series of commands can be stored in computer memory and given to the motors at predetermined times in order to create a pattern of motion for the sample.

The Motion Control system works along side the Fluid System. The Fluid System begins with a Harvard Apparatus Series 11 Plus Advanced syringe pump. This pump is fitted with a 100 μL Hamilton Gas Tight 1700 series syringe for extractions, and either a 10 μL 1800 series or 0.5 μL 7000 series syringe for spot deposition, described below. According to the manufacturer, with this size of syringe, the pump is capable of infusing or withdrawing anywhere from 0.0049 μL/min to 79.41 μL/min. The syringe is attached to microbore Tygon tubing with an inner diameter of 0.25 mm, which has a volume of 0.5 μL per cm of length. The tubing is in three sections, connected by a Y-piece connector from LabSmith, with a dead volume of 0.1 μL. One branch of the tubing is connected to the syringe, while the other two are connected to input and output needles, with each needle having a dead volume of about 2.5 μL. Between the T-piece and the needles is a 3 way pinch valve, which will close either the input or output channel while

leaving the other open. This system has a total dead volume of roughly 7 μL in each branch. The entire system is shown schematically in figure 5.

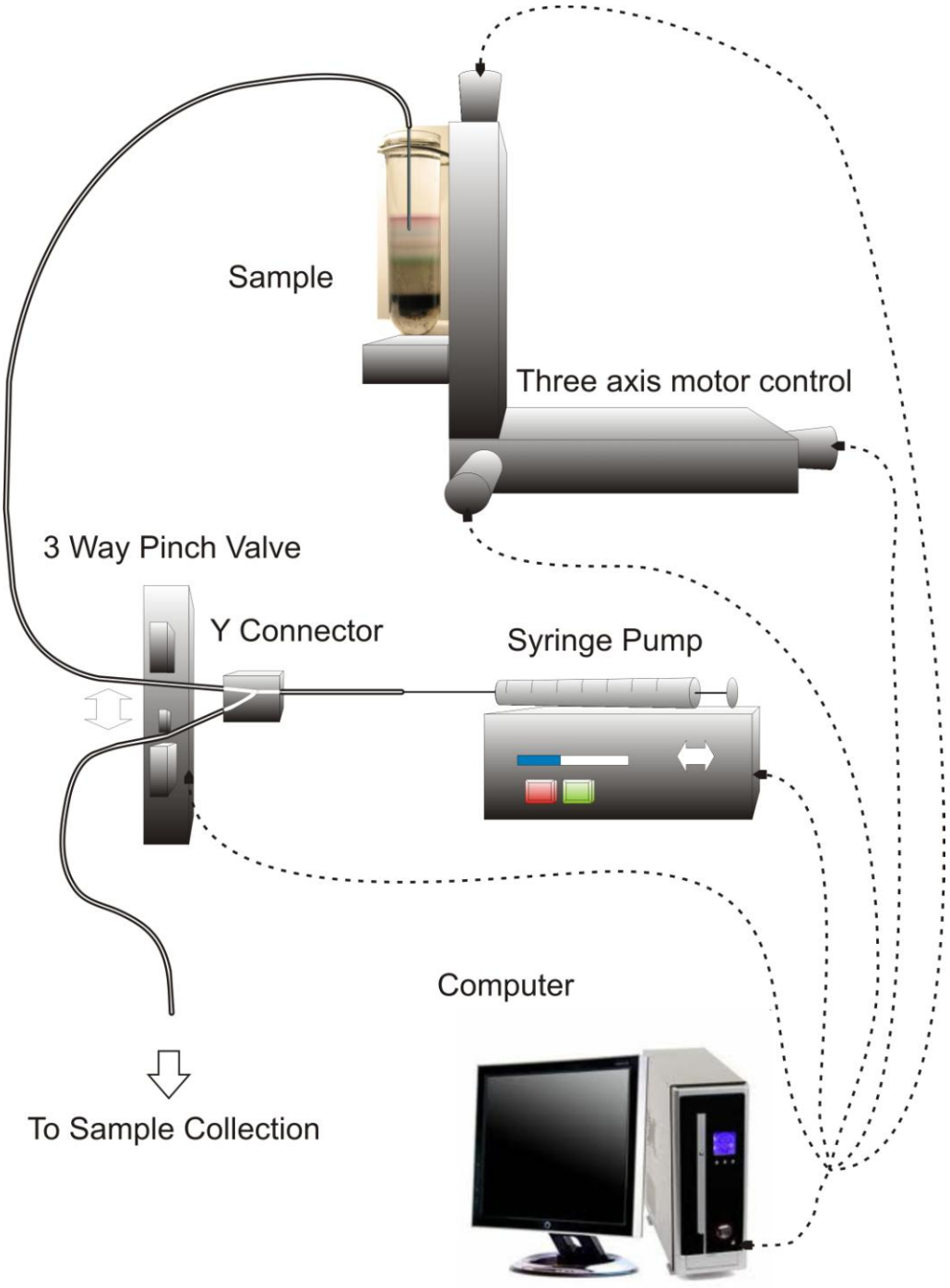

Figure 5. Schematic drawing of the Fractionator. The fluid extraction system works in conjunction with the motion control system to effectively extract enriched sample from a DGU separation

3. Experimental Procedure - Extraction

From start to finish, the extraction procedure is as follows. First, a DGU sample is prepared according to the procedure by Ghosh et al.[7] Once the DGU sample has finished separating, it is necessary to determine the positions of each band to be extracted. This is done by depth resolved fluorescence spectroscopy. A 638 nm laser is passed through the sample at a specific height, and the resultant fluorescence intensity is measured. The height of the sample is adjusted so that the laser scans through the complete region of interest, allowing the position of each band to be determined. This information is then entered into the sample collection software, along with user selected values for the speed of the motors, rate of extraction, and the number of passes per band. Next the needle is brought to the first target depth. The motors then begin their automated movement pattern, typically an Archimedean Spiral, while the syringe pump begins extracting. An Archimedean Spiral was chosen as the circular analog to a raster scan. This motion and extraction continues until one of two triggers occurs. Either the syringe fills with sample, at which point the motion stops and the sample is ejected into a collection vial, or the prescribed motion is completed. When the motion is completed, the sample is lowered until the needle is in a region of the sample with no SWCNTs. At this point, the pump extracts some blank sample to wash the tubing to ensure minimal mixing. The program then moves the sample so that the needle is positioned at the next target depth, or returns to the beginning if it has already extracted all target layers. Figure 6 shows a simplified flow chart of the Fractionator control program.

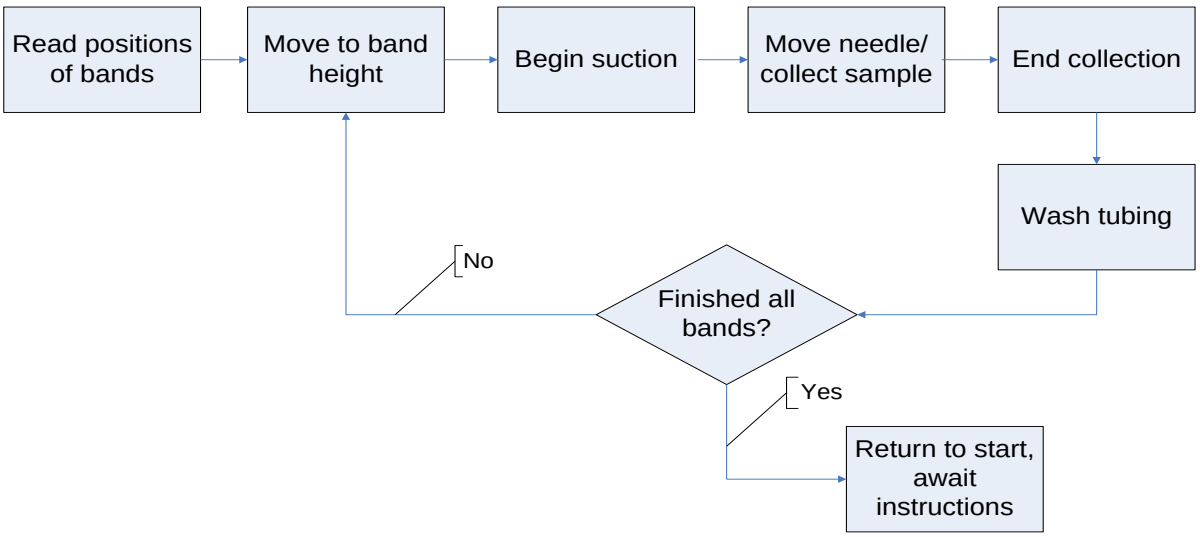

Figure 6. Simplified flow chart of Fractionator extraction process.

In order to fully characterize the performance of the Fractionator, fluorescence spectra of extracted fractions were taken with multiple excitation wavelengths of 638, 642, 659 and 784 nm. Absorption spectra were also taken in the visible and near-IR regions. The fluorescence intensity as a function of emission and excitation wavelength was measured using a J-Y Spex Fluorolog 3-211 described more fully in appendix A. An example of a typical enriched sample obtained using this procedure is shown in figure 7.

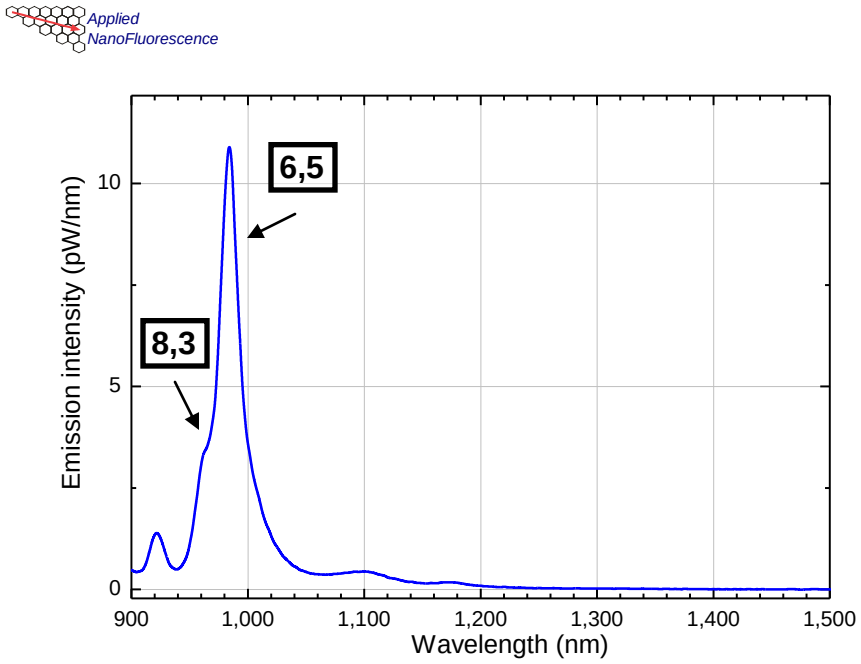

Figure 7. A fluorescence spectrum of a representative example of a sample extracted by the Fractionator. This is a sample enriched in (*6,5*) SWCNTs. (*8,3*) and (*9,1*) tubes are the most significant impurities. 784 nm excitation.

4. Experimental Procedure – Absorption Cross Section Determination

In order to determine the absorption cross section, the total absorption from the target analyte and the concentration of that analyte must be determined experimentally. Our experiments begin by performing absorbance measurements on a (*6*,*5*) enriched sample obtained from the procedure stated above. Our method for determining the concentration is straightforward, and involves using the Fractionator to deposit a small volume of (*6*,5) enriched SWCNT suspension onto a polycarbonate cover slip. The droplets are allowed to dry, which causes the suspended SWCNTs inside to adhere to the polycarbonate surface. The cover slip is then attached to a quartz slide, and the spot is imaged using a near-IR fluorescence microscope setup described in detail in appendix A. In short, the microscope is capable of capturing images or videos of SWCNT fluorescence while the sample is being excited by a laser. In order to achieve a useful SWCNT number density for the microscopy, the as-collected sample was diluted by a factor of 20,000 with a solution of 30% by volume isopropanol in water. The isopropanol was added to inhibit the so-called "coffee ring effect"[14] where the majority of the tubes deposit at the edge of the droplet while it dries. Such coffee rings made distinguishing between individual tubes impossible with our current optical resolution. The isopropanol works by lowering the surface tension of the liquid, allowing Marangoni flow to recycle the SWCNTs back towards the center of the drop as it dries.[15] The ratio of 30% isopropanol by volume was chosen for practical reasons: at higher concentrations, the

isopropanol disrupts the polymer of the polycarbonate coverslip, making imaging impossible; while at lower concentrations the coffee ring of SWCNTs remains.

In order to determine the exact volume of the droplet deposited onto the polycarbonate coverslip, 2 calibration methods were used. The first was to measure the position of the plunger stage on the syringe pump before and after depositing nominally 8 nL 200 times. The second method was to deposit nominally 8 nL of 26 % NaCl solution onto an aluminum foil disk. The water in this solution was driven off by heating the disk to 170˚ C under an inverted Petri dish. The mass of salt deposited was then measured and used to calibrate the volume deposited with each drop.

For our microscopy experiments, 840 nm light from a Ti:Sapphire laser was used to excite the first vibronic sideband of the E_{11} transition of (*6*,5) tubes in the sample. After a spot from a dried drop was located, videos were recorded in a raster scan pattern until the whole spot was imaged, since the spot was much larger than the microscope's field of view. Each video was 75 frames long with an integration time of 0.5 seconds per frame. The raster scan was done using two stepper motors to control the motion of the slide and coverslip, giving precise and repeatable control, and eliminating double counting. After the videos were taken, they were analyzed by a program that was based on a program described in detail elsewhere.[16] The program used for this study closely follows the original version, but does not need to analyze the motion of the tubes. In addition, certain variables were re-optimized for the parameters of this study. After all the videos were processed, the total number of tubes was used to calculate the carbon atom number density in the original solution, using the average length of (*6*,5) SWCNTs in the

sample. The average length was measured using the technique described in the previous reference.

5. Results

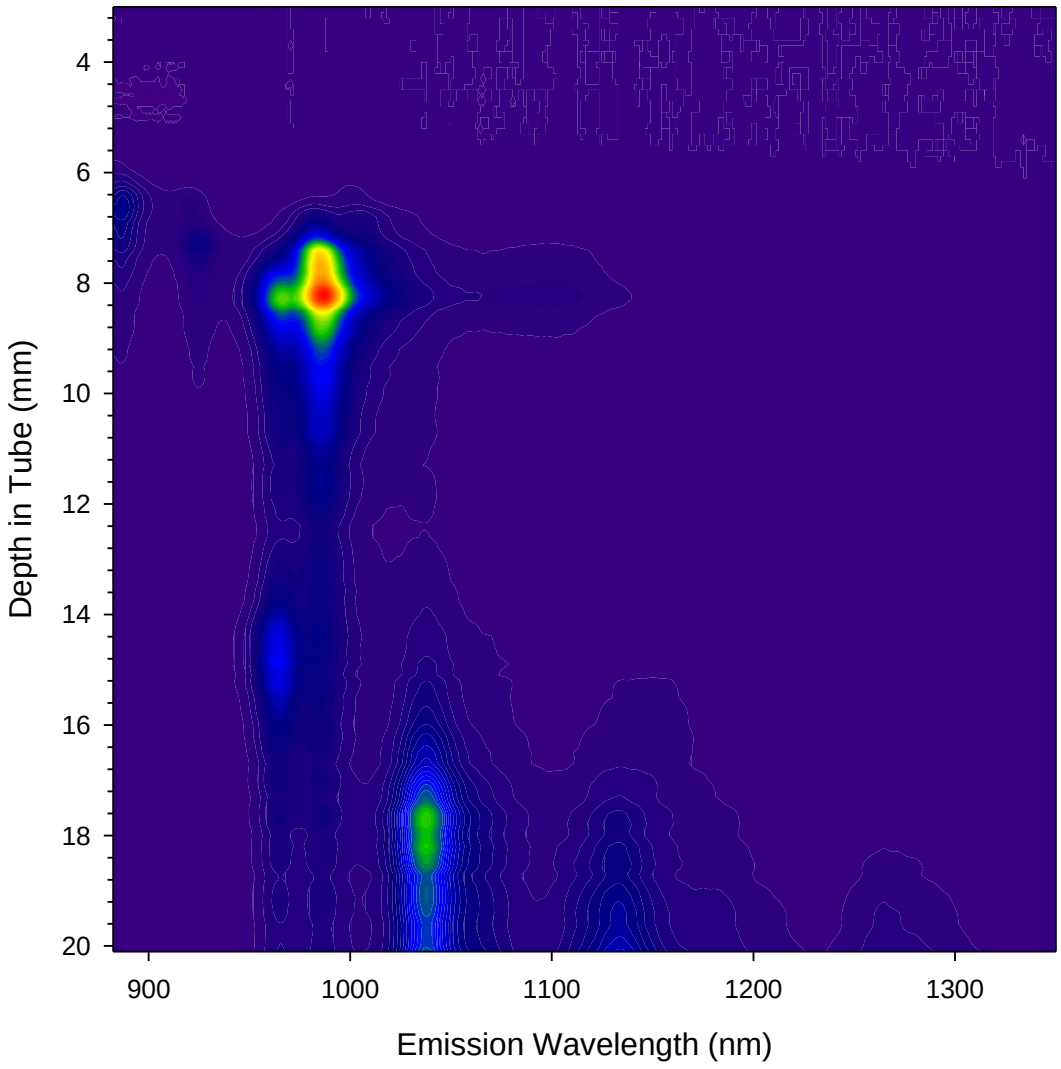

Figure 8. Depth Resolved Fluorescence of a DGU separation. Extraction took place on this sample at 7.5 mm and 18 mm depth. 638 nm excitation.

Figure 7 shows the depth resolved emission profile of a centrifuge tube after DGU separation. Note that in this separation, the density gradient was made such that the (*7*,*6*) band is not visible. The (*6*,*5*) band was targeted for extraction at a depth of 7.5 mm, while the (*7*,*5*) band was targeted at 18 mm. The Fractionator was set to collect at a rate of 25 μL/min with a fixed speed of 0.5 mm/sec for each motor. Each band was extracted in three passes. This resulted in roughly 150 μL of collected sample for each species, and took roughly 5 minutes per band. Absorption and fluorescence spectra were measured. The results for the (*6*,*5*) sample are shown in figures 8 and 9.

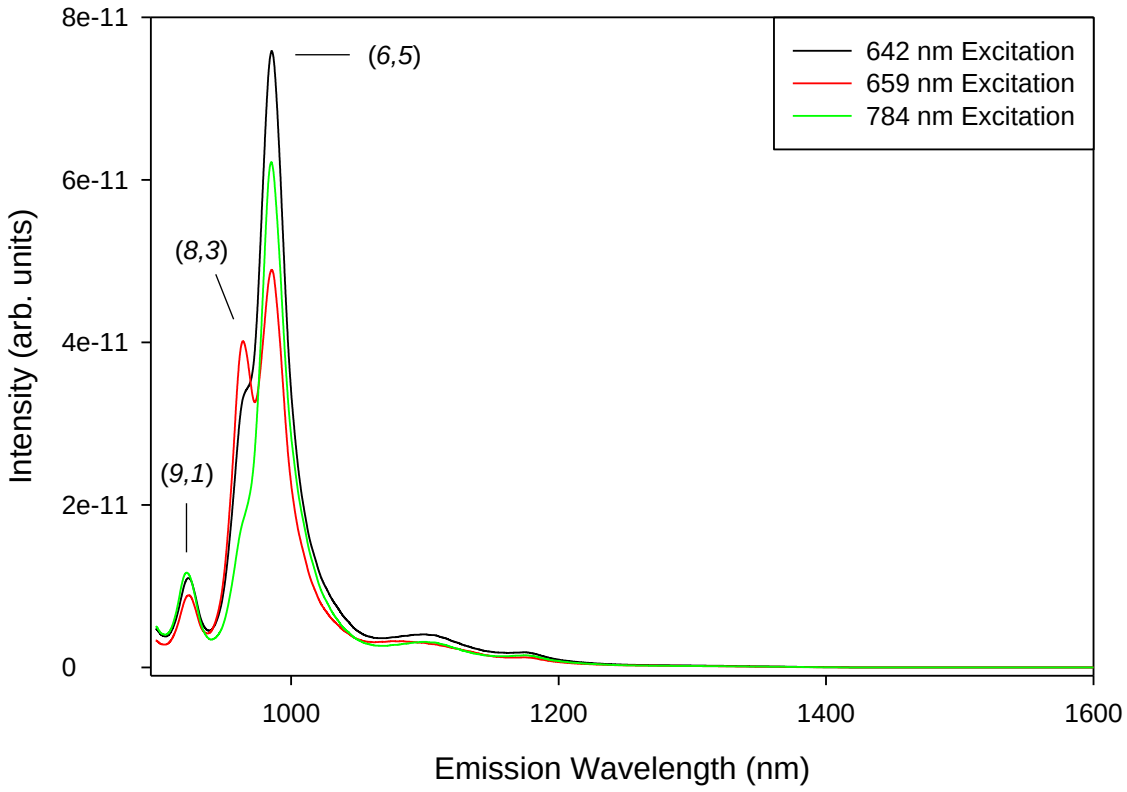

Figure 9. Fluorescence Emission spectra for the collected (*6*,*5*) sample. These spectra confirm the degree of enrichment of the collected fraction.

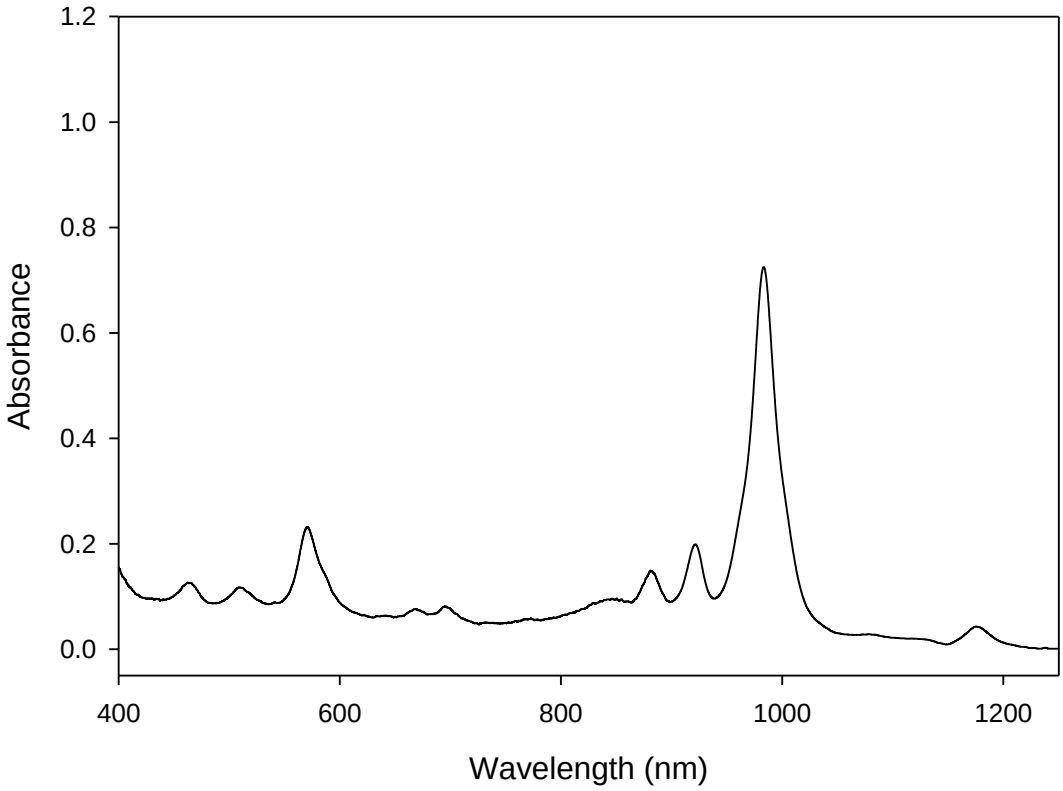

Figure 10. Absorption Spectra of the (*6*,*5*) sample.

One performance measure of the Fractionator is the degree to which it preserves the separation present in the post-DGU sample. To assess that, it is possible to compare the fluorescence at the target depth with the final extracted sample. Figure 10a and 10b show the comparisons for the (*6*,*5*) and (*7*,5) samples, respectively. These figures are representative of samples extracted using the Fractionator. The fluorescence spectra from figure 8 can be used to estimate the percent composition of the sample, as detailed elsewhere.[17] In this method, the following model is used to describe the fluorescence from the each laser from each nanotube species:

$$S^{i}_{n,m}(\nu_{em}) = F_{instr}(\nu_{em}) \cdot [C]_{n,m} \cdot P(\nu^{i}_{exc}) \cdot \sigma_{rel}(\nu^{i}_{exc})_{n,m} \cdot f_{n,m}(\nu_{em} - \nu_{n,m}) \cdot (\sigma_{22}\Phi_{Fl})_{n,m} \quad (4)$$

where $S^{i}_{n,m}(\nu_{em})$ is the fluorescence intensity at frequency ν_{em}; $F_{instr}(\nu_{em})$ is the instrument collection efficiency and response function at ν_{em}; $[C]_{n,m}$ is the carbon concentration of the species in question; $P(\nu^{i}_{exc})$ is the photon irradiance at the sample from the *i*th laser; $\sigma_{rel}(\nu^{i}_{exc})_{n,m}$ is the ratio of the absorption cross section at the excitation wavelength to the E_{22} absorption cross section; $f_{n,m}(\nu_{em} - \nu_{n,m})$ is the area normalized emission line shape function for the (*n,m*) species centered at $\nu_{n,m}$; and lastly, $(\sigma_{22}\Phi_{Fl})_{n,m}$ is the photoluminescence action cross section, defined as the product of the quantum efficiency and the absorption cross section for the (*n,m*) species. The total fluorescence intensity is the sum of each constituent signal:

$$S^{i}_{total}(\nu_{em}) = \sum_{(n,m)} S^{i}_{n,m}(\nu_{em}) \quad (5)$$

This allows for the estimation of $[C]_{n,m}$ using 3 different spectra, when the other variables are well known.

Unfortunately, this model does not include the long wavelength asymmetrical tail present in the emission spectra of SWCNTs. When many species are present together, this tail becomes buried in the spectral congestion. However, in our enriched samples, these tails are significant, and contribute to the spectral line shape. However, it is also likely that there is the presence of other species of tubes which emit at just slightly longer

wavelengths than the dominant peak. For the (*6,5*) sample shown here, that is the (*7,3*) species. However, since the model, when used with three excitation wavelengths is unable to distinguish the long wavelength tail from the contribution of this minor species, it attributes both effects to the presence of the (*7,3*) tubes. Thus, the percent composition graph shown in figure 11 represents a 'worst case scenario', and the (*6,5*) percent composition is at least 50%, but may be as high as ~70%.

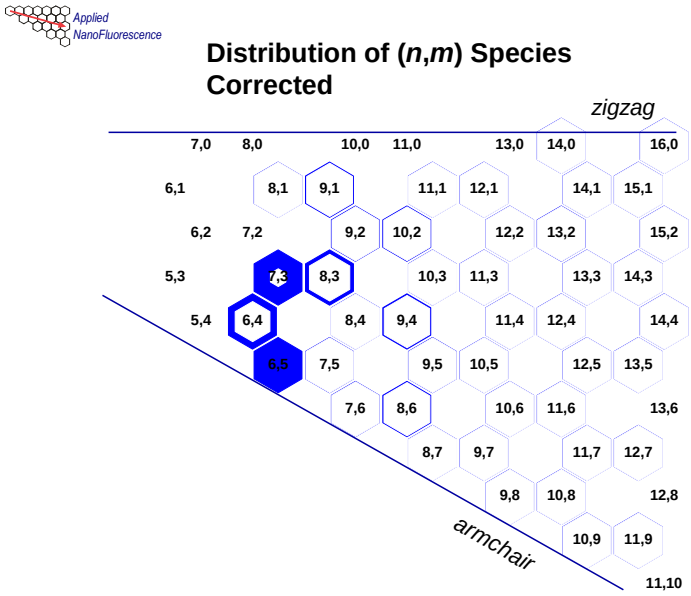

Figure 11. Estimated relative abundance of tube species in the (*6,5*) enriched sample. Note that there may be an overestimation of the (*7,3*) peak due to the long wavelength tail of the (*6,5*) peak.

To get another view of the actual sample composition, fluorescence intensity as a function of both excitation and emission wavelength are displayed in figure 12. This figure shows that the total (*7,3*) peak height is small, despite what an estimated fluorescence action cross section nearly equal to that of (*6,5*) tubes[18].

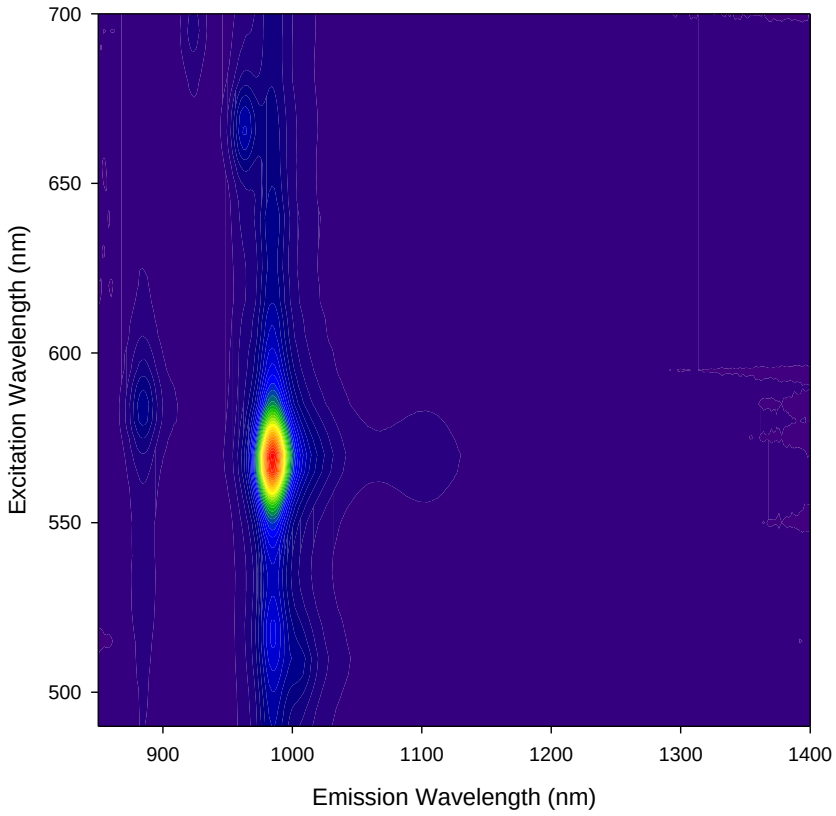

Figure 12. Fluorescence intensity as a function of emission and excitation wavelength. The (*6,5*) peak is the dominant peak, while the (7,3) peak appears only at excitation wavelengths close to its resonance of 505 nm. The (*8,3*) and (*6,4*) bands are also present. The estimated ratio of (*6,5*) to (*7,3*) is ~5:1.

In addition, figure 13 shows the fluorescence signal for the entire depth of the separated sample at two important wavelengths. The (*6,5*) tubes should fluoresce at 985 nm, while the (*7,3*) tubes should fluoresce at 1000 nm. The dots in the figure are drawn as a guide to the eye to indicate the depth at which the extraction took place. As one can see, the majority of the signal at 1000 nm is from the (*6,5*) peak, since for most of the depth, the two line shapes are nearly identical. However, it can be seen that at smaller depths than the (*6,5*) peak, the (*7,3*) band makes a contribution to the fluorescence at 1000 nm. These two pieces of evidence seem to indicate that at the extraction position, the (*7,3*)

band has already passed, and should not make a large contribution to the population of the extracted sample.

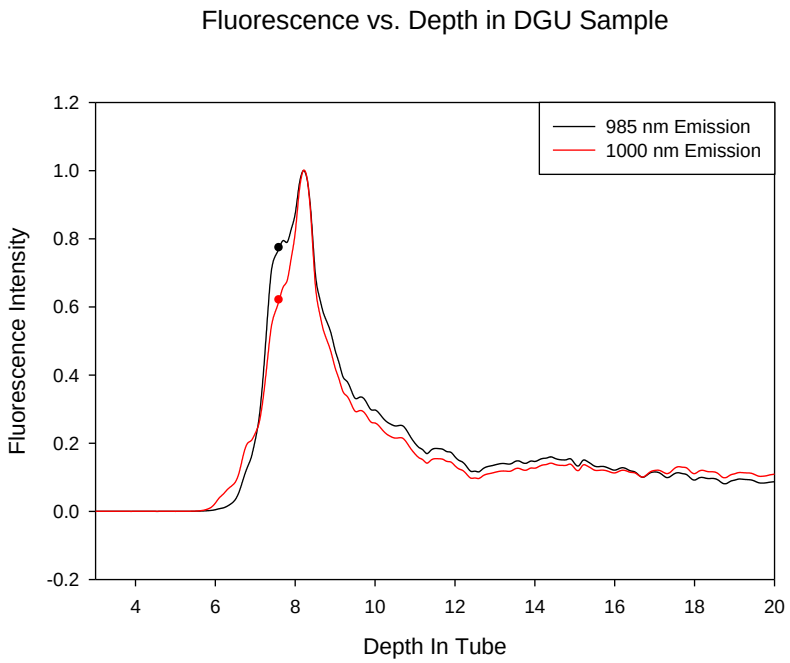

Figure 13. Fluorescence Emission as a function of depth in the tube. This plot serves to illustrate that at the height where extraction took place, the signal at 1000 nm was from the (*6*,*5*) tubes, not (*7*,*3*). Because 1000 nm is the emission resonance for (*7*,3), this supports the idea that the (*7*,*3*) species is not a major component of the collected sample. The dots are a guide to the eye to indicate where the extraction took place.

Figure 14. Microscopic image of tubes deposited on a polycarbonate cover slip. These tubes are being excited by 840 nm laser light, and their fluorescence is detected as the signal. This image is the average of 75 individual images.

The (*6*,*5*) absorbance peak was determined from the spectrum in figure 10. The analysis assumed no background, which necessarily precludes the presence of metallic or semi-metallic tubes. The validity of this assumption is discussed below. Figure 14 shows an example of a microscopic image of part of one of the sample deposits. Each bright spot is a nanotube, although not all the nanotubes are immediately visible as bright spots in this frame, due to low intensity from blinking or a high defect density. Over many frames, however, these spots become detectable, since blinking is temporary, and the noise surrounding any dim tube will average out to 0, while the signal from the tube will stay above the noise threshold. Seven deposits were analyzed, each with roughly 10

videos worth of area. The average number of tubes per spot was 334 ± 93. The calibration of the deposition method indicated that the average spot size was 12 μL. The measured value for the average length of the nanotubes was 326 nm. The calculated value for the absorption cross section is therefore $9.2 \pm 2.6 \times 10^{-17}$ cm^2 C $atom^{-1}$.

6. Conclusion

We have constructed an instrument capable of extracting samples enriched in just a few (*n*,*m*) species of nanotubes from a DGU separated sample. This instrument is capable of quickly extracting samples while preserving the sorting created by the DGU. It is capable of performing this extraction in a fully automated manner. The purity of the extracted sample is not as high as is desirable, but it appears that this is a limitation of the DGU process, rather than mixing during the extraction. It is important to improve the DGU separation as much as possible to fully demonstrate the potential of the Fractionator, but the early results are promising. There are many fundamental unknown relationships in SWCNT research, and much of that is because of the lack of high purity samples. This instrument will open new avenues for study, similar to one recently conducted by Ghosh et al. in which a high purity sample was essential to the discovery of O-doped SWCNTs whose fluorescence signal would have been hidden otherwise.[19]

With respect to the determination of absorption cross sections, much work remains before the results can be considered conclusive. At this point, the random errors appear to be acceptable, with the variance in the final value probably dominated by

variations in the spot size. This variation should decrease with increased familiarity with the experimental procedure on the part of the experimenter. However, more work remains to exclude systematic errors in the study. Our (*6,5*) cross-section value is significantly higher than previous reports. This might correspond to detecting fewer tubes per unit volume. The main routes through which this might occur are aggregation on the polycarbonate surface and the inability to detect all nanotubes using the microscope.

In our experiment, as the deposit dries to form a spot on the slip, tubes can deposit on top of one another to form loose aggregates because the concentration of surfactant is so low that there is likely none remaining on the tubes themselves. These surface aggregates can either be homogenous or heterogeneous with respect to nanotube species. Homogenous aggregates will still fluoresce; while heterogeneous aggregates should have their fluorescence quenched by inter tube energy transfer which leads to non-radiative relaxation. However, even if a surface aggregate is made up of one single species of tube and still fluorescent, there is no way in our experiment to determine how many individual tubes make up the surface aggregate. Thus, we can, at most, count each aggregate as 1 nanotube, decreasing our total count of nanotubes relative to the true value.

Additionally, there are likely tubes which have been deposited onto the microscope coverslip but are not detectable by the microscope. This can occur when the tubes contain a high enough defect density that their fluorescence is below the noise threshold, and cannot be separated from the background. Another possible source of deterministic error is overestimation of the absorbance peak. While our lack of inclusion of a background in the analysis of the spectrum is an assumption, it has been tested previously on samples enriched in one species, and found to be a good assumption.[20]

Future work will mainly focus on testing and eliminating the sources of such systematic errors. More studies need to be done on the effect the dilution factor has on the final calculated absorption cross section value. Previous work was conducted, but it needs to be repeated with recent upgrades to the experimental system. The solution used to dilute the as collected sample for deposition does not contain any cholate. This is because at the concentrations used in the DGU process (0.7% w/v), the surfactant forms a film on the cover slip which obscures tubes makes imaging and counting impossible. However, even at sodium cholate concentrations as low as 0.02% w/v the micelles can remain stable. If the dilution is carried out with a water-alcohol solution with 0.02% sodium cholate, the tubes may be inhibited from depositing on top of one another, due to Coulomb repulsion of the negatively charged outer surfaces of the micelles. Further testing is required to determine if this concentration of sodium cholate forms the same film on the cover slip surface.

In addition, one alternative experiment is proposed. In this method, instead of depositing a small volume of sample and attempting to image the entire spot, only a fraction of the volume deposited needs to be imaged. This is accomplished by diluting the tube solution with an agarose solution, instead of water. This tube-agarose solution can then be deposited onto specially prepared quartz slides that contain chemically etched wells. The height of these wells is well characterized, and crucially, is smaller than the focal depth of the microscope. This means that the entire height of the well can be focused at the same time, and thus the entire depth of the well can be imaged at once. Using the depth of the well and the X and Y dimensions of the detector, the volume represented in each image can be calculated. Thus, each image has a known volume of

sample, and a countable number of tubes. With enough images, good statistics could be determined from the sample. Not only does this method not require imaging the entire sample, but it also has the benefit of not requiring deposition of nanoliter sized volumes, and inhibiting aggregation, as the agarose gel should form before aggregation can occur in our concentration range. The drawback to such a method, of course, is that it relies very heavily on the ability to image the entire depth of the sample at once. If this is not possible, this experiment would not be viable without further adjustment. It is also necessary to know to a high degree of precision, the height of the well, plus any overflow that occurs, since there will always be some gel solution between the top of the slide and the coverslip. Estimating this overflow will require additional experiments, and may be a source of error.

Once the experimental procedure is refined for the (*6,5*) sample, the experiment will be expanded to include (*7,5*), (*7,6*), and (*8,3*) tubes. These tubes are the major species present in our HiPco samples. The experimental determination of these values would be a large step forward in the ability to clear away some of the guesswork involved in the optical study of mixed samples.

Appendix A – Instrumental Details

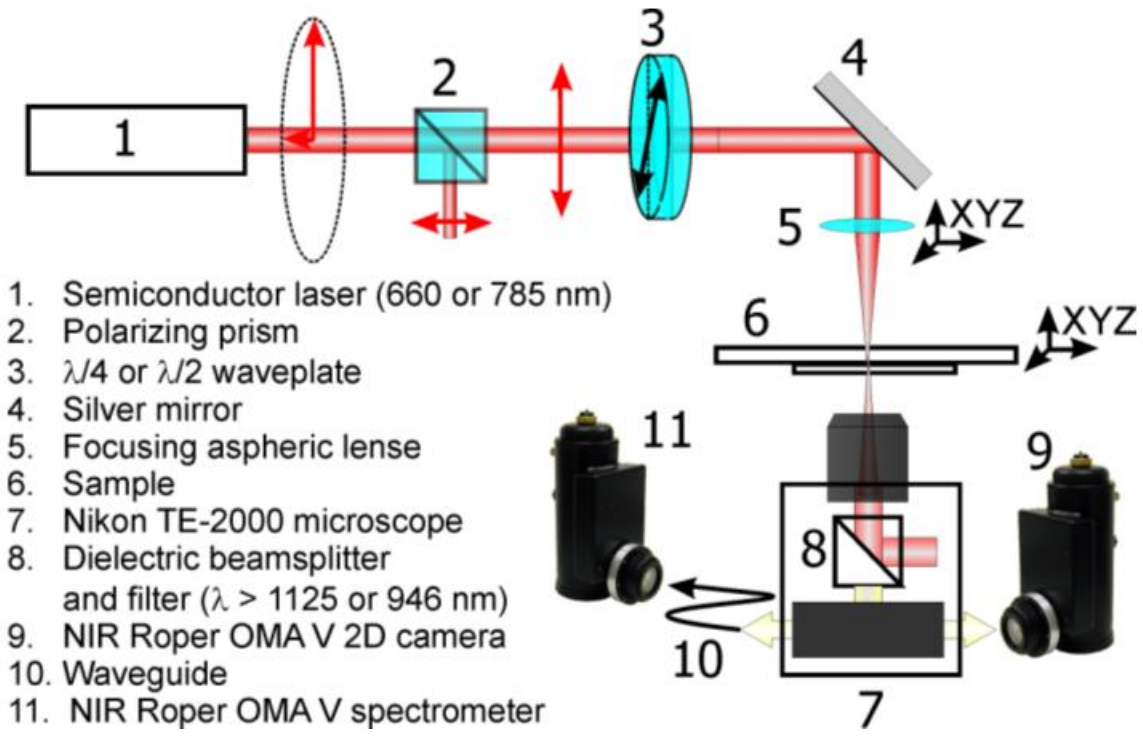

Figure A1-1. Diagram of the setup used in microscopy experiments in this study.[21]

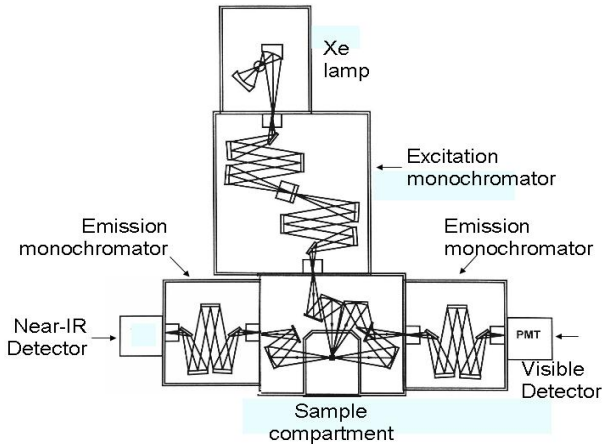

Figure A1-2. Diagram of the J-Y Spex Fluorolog 3-211. Emission monochromator was set to 6 nm width, excitation monochromator was set to 8 nm width.

Appendix B – Density Gradient Ultracentrifugation Experimental Details

Procedure follows from that by Ghosh et al.[7] A SWCNT slurry was prepared by adding 5 mg of raw SWCNTs (HiPco process, Rice University, batch 188.1) to 10 mL of 2% sodium cholate solution. This slurry was bath sonicated (Sharpertek Stamina XP) for one hour and tip sonicated (Misonix Microson XL) at 7 W for 30 minutes. The resulting solution was centrifuged at 13,330*g* (Biofuge-13, Baxter Scientific) for 30 minutes to pellet out iron catalyst and any remaining nanotube bundles.

The density gradient was formed using iodixanol, purchased as a 60% (w/v) solution from Sigma-Aldrich. Seven different solutions containing 0.7% sodium cholate and varying concentrations of iodixanol were prepared from this stock. The solutions were layered into a 5.0 mL capacity centrifuge tube (Seton Scientific 7022) in the following order by % Iodixanol and volumes: 30% (500 μL); 27.5% (420 μL); 25% (540 μL); 22.5% (660 μL); 20% (660 μL); 17.5% (720 μL); and 15% (780 μL). This layered solution was allowed to form a smooth density gradient with 1 h of diffusion. The SWCNTs were inserted into the density gradient by mixing 525 μL of SWCNT-cholate solution with 325 μL of 60% iodixanol solution. This solution was slowly pipetted into the density gradient.

The centrifuge tube was then placed into a MLS-50 swing bucket rotor, which was placed into a Beckman Optima Max (Model MAX 130k) ultracentrifuge. The rotor was spun at 50,000 r.p.m. to subject the tube to 268,000*g*. The temperature was set to 22˚ C. After 18 hours, the separation was complete, and the sample ready to be characterized and fractionated.

References

(1) Iijima, S. *Nature* **1991,** *354*, 56-58.

(2) Radushkevich, L. V.; Lukyanovich, V. M. *Soviet Journal of Physical Cemistry* **1952,** *26*, 88-95.

(3) Ajayan, P. M.; Zhou, O. Z. *Carbon Nanotubes : Synthesis, Structure, Properties, and Applications [Figures] [Plates]*. *CARBON NANOTUBES*, SYNTHESIS.

(4) Bachilo, S. M.; Strano, M. S.; Kittrell, C.; Hauge, R. H.; Smalley, R. E.; Weisman, R. B. *Science* **2002,** *298*, 2361-2366.

(5) Zheng, M.; Jagota, A.; Strano, M. S.; Santos, A. P.; Barone, P.; Chou, S. G.; Diner, B. A.; Dresselhaus, M. S.; Mclean, R. S.; Onoa, G. B.; Samsonidze, G. G.; Semke, E. D.; Usrey, M.; Walls, D. J. *Science* **2003,** *302*, 1545-1548.

(6) Arnold, M. S.; Stupp, S. I.; Hersam, M. C. *Nano Lett.* **2005,** *5*, 713-718.

(7) Ghosh, S.; Bachilo, S. M.; Weisman, R. B. *Nature Nanotech.* **2010,** *5*, 443-450.

(8) Nair, N.; Kim, W. J.; Braatz, R. D.; Strano, M. S. *Langmuir* **2008,** *24*, 1790-1795.

(9) Islam, M. F.; Milkie, D. E.; Kane, C. L.; Yodh, A. G.; Kikkawa, J. M. *Phys. Rev. Lett.* **2004,** *93*, 037404-1-037404-4.

(10) Zheng, M.; Diner, B. A. *J. Am. Chem. Soc.* **2004,** *126*, 15490-15494.

(11) Berciaud, S.; Cognet, L.; Lounis, B. *Phys. Rev. Lett.* **2008,** *101*, 077402-1-077402-4.

(12) Matsuda, K.; Kanemitsu, Y.; Irie, K.; Saiki, T.; Someya, T.; Miyauchi, Y.; Maryama, S. *Appl. Phys. Lett.* **2005,** *86*, 12316-1-12316-3.

(13) Schöppler, F.; Mann, C.; Hain, T. C.; Neubauer, F. M.; Privitera, G.; Bonaccorso, F.; Chu, D.; Ferrari, A. C.; Hertel, T. *J. Phys. Chem. C* **2011,** *115*, 14682-14686.

(14) Deegan, R. D.; Bakajin, O.; Dupont, T. F.; Huber, G.; Nagel, S. R.; Witten, T. A. *Nature* **1997,** *389*, 827-829.

(15) Hu, H.; Larson, R. G. *J. Phys. Chem. B* **2006,** *110*, 7090-7094.

(16) Streit, J. K.; et al. *Unpublished Results* **2011**.

(17) Rocha, J.-D. R.; Bachilo, S. M.; Ghosh, S.; Arepalli, S.; Weisman, R. B. *Anal. Chem.* **2011,** *83*, 7431-7437.

(18) Tsyboulski, D.; et al. *Unpublished* **2011**.

(19) Ghosh, S.; Bachilo, S. M.; Simonette, R. A.; Beckingham, K. M.; Weisman, R. B. *Science* **2010,** *330*, 1656-1659.

(20) Naumov, A. V.; Ghosh, S.; Tsyboulski, D. A.; Bachilo, S. M.; Weisman, R. B. *ACS Nano* **2011,** *5*, 1639-1648.

(21) Tsyboulski, D. A.; Bachilo, S. M.; Weisman, R. B. *Nano Lett.* **2005,** *5*, 975-979.